Materials Research Bulletin 171 (2024) 112609

Contents lists available at ScienceDirect

Materials Research Bulletin

journal homepage: www.elsevier.com/locate/matresbu

Research Papers

Radiation response properties of Ce-doped CaF_2 transparent ceramics

Naoki Kawano [a,*], Takumi Kato [b], Robin L. Conner [c], Luiz G. Jacobsohn [c], Daisuke Nakauchi [b], Yuma Takebuchi [b], Hiroyuki Fukushima [d], Daiki Shiratori [e], Takayuki Yanagida [b]

[a] Graduate School of Engineering Science, Akita University, 1-1Tegata Gakuen-machi, Akita 010-8502, Japan
[b] Graduate School of Science and Technology, Nara Institute of Science and Technology, 8916-5 Takayama-cho, Ikoma, Nara 630-0192, Japan
[c] Department of Materials Science and Engineering, Clemson University, 515 Calhoun Dr, Clemson, SC, 29634, United States
[d] National Institute of Technology, Fukui College, Geshi-cho, Sabae, Fukui 916-8507, Japan
[e] Faculty of Engineering, Tokyo University of Science, 6-3-1 Niijuku, Katsushika, Tokyo 125-8585, Japan

ARTICLE INFO

Keywords:
Ce^{3+}
Transparent ceramic
CaF_2
Scintillator
Luminescence

ABSTRACT

We report on the luminescence properties of CaF_2 transparent ceramics having various concentrations of CeF_3 (0.1 %, 0.5 %, and 1 %). Scintillation emissions centered at approximately 318, 345, and 386 nm derived from the 5d→4f transition of Ce^{3+} were detected, and scintillation light yields were determined to be 8600 photons/MeV (0.1 % CeF_3), 1930 photons/MeV (0.5 % CeF_3), and 1850 photons/MeV (1 % CeF_3) under gamma-ray irradiation from ^{241}Am. The Ce-doped CaF_2 transparent ceramics showed thermally stimulated luminescence (TSL) with a broad glow peak at around 115–145 °C, and their dose response curves were determined over a broad dose range (0.01–3 mGy). Moreover, optically stimulated luminescence (OSL) exponential decay curves were obtained under 500 nm stimulation light, and dose response curves were obtained in the dose range of 0.1–100 mGy. The minimum detectable dose was estimated to be 0.1 mGy. A direct correlation between scintillation light yields under gamma-ray irradiation and TSL/OSL intensities was demonstrated.

1. Introduction

Radiation detectors based on phosphor materials have received considerable attention in many applications such as new oil reserves exploration, medical diagnostic imaging, environmental radiation monitoring, and border security systems [1–5]. Scintillators have the function of transforming each high energy photon into tens of thousands of ultraviolet-visible photons that are efficiently detected by photodetectors. The requirements for a scintillator include high density, low fabrication cost, high radiation tolerance, high light yield, chemical stability, low afterglow, and a fast decay time, with the requirement priorities depending on the specifics of each application [6]. Another type of phosphor material used for the measurement of ionizing radiation are luminescence dosimeters. They can store a fraction of the radiation energy in the form of trapped charges for several weeks and then emit light in the form of ultraviolet-visible photons when under thermal (thermally stimulated luminescence; TSL) or optical (optically stimulated luminescence; OSL) stimulation. The required features for these materials include low fading of the stored signal, high luminescence intensity, high chemical stability, and dose linearity [7]. Recently, a complementary correlation between scintillation and dosimetric properties has been demonstrated in several compounds; therefore, both sets of characteristics should be investigated for the same phosphor to achieve a higher level of understanding of the interaction of ionizing radiation and the luminescence response [8,9,10].

CaF_2 is used for scintillation and dosimetry applications. This material is known to have a large bandgap energy (about 12 eV), high chemical stability, and low phonon energy [11–12]. It is available as a natural crystal and it can be fabricated in large size and quantities. Undoped CaF_2 crystal shows self-trapped exciton (STE) luminescence with a broad band centered at approximately 270 nm, and its scintillation light yield is 13,000 photons/MeV under ^{137}Cs gamma-ray irradiation [12]. Furthermore, Eu-doped CaF_2 crystals have a high light yield of 24,000 photons/MeV, and they are considered for use in the search on dark matter in astrophysics research since the presence of ^{19}F is advantageous for spin coupled dark matter search [13]. Eu-doped CaF_2 nanoparticles have also been investigated and the scintillation mechanism discussed in detail [14–16]. Moreover, CaF_2 has low effective atomic number (16.5); therefore, it can be employed for dosimetric applications given its bioequivalence. For instance, Mn-doped CaF_2 is

* Corresponding author.
E-mail address: n-kawano@gipc.akita-u.ac.jp (N. Kawano).

https://doi.org/10.1016/j.materresbull.2023.112609
Received 10 August 2023; Received in revised form 26 October 2023; Accepted 8 November 2023
Available online 10 November 2023
0025-5408/

used for dosimetry and commercially known as TLD-400 [17]. Its dynamic range is from 0.1 μGy to 100 Gy, and TLD-400 can be used for environmental radiation monitoring and high dose measurements. Moreover, Dy-doped CaF_2 is employed in TLD-200 dosimeters [17]. Its useful dose range is from 0.1 μGy to 10 Gy and is commonly used for environmental radiation monitoring.

Transparent ceramics have attracted much attention due to several industrial advantages including greater shape control, fast and low cost fabrication method, and homogeneity of the dopants [18–25]. Recently, special effort has been focused on fluoride ceramics [26–27]. CaF_2 transparent ceramics have been synthesized by several methods, including spark plasma sintering (SPS) [28–29]. For example, a highly transparent ceramic was prepared by N. Guo et al. via a cold sintering process with its transmittance being about 82 % in the visible range [29]. Moreover, our group has reported the luminescence properties of several CaF_2 transparent ceramics with an activator [30–33]. In particular, the Eu^{2+}-doped CaF_2 transparent ceramics showed efficient scintillation (approximately 18,000 photons/MeV), a linear TSL dose response over the broad range of 0.1–1000 mGy, and the observation of OSL [30]. In this work, we synthesized CaF_2 transparent ceramics with various CeF_3 concentrations (0.1 %, 0.5 %, and 1 %) by SPS for the investigation of the response to ionizing radiation. Ce^{3+} ions were chosen since the Ce^{3+} ion is a well-known fast luminescence center in the ultraviolet/visible region compatible with standard instrumentation for ionizing radiation measurements, while the lifetime of Eu^{2+} in CaF_2 has been reported to be 900 ns [34]. Also, Ca^{2+} ions in the CaF_2 host can be easily replaced with Ce^{3+} ions since the ionic radius of Ca^{2+} (1.12 Å) is close to that of Ce^{3+} (1.14 Å) [35]. Herein, we investigated the photoluminescence, scintillation, and TSL/OSL properties of Ce^{3+}-doped CaF_2 transparent ceramics for scintillation and dosimetry applications.

2. Experimental methods

The synthesis of the undoped and Ce-doped CaF_2 transparent ceramics was performed as follows. 99.99 % purity powders of CaF_2 and CeF_3 from Stella Chemifa were mixed in different molar ratios (0, 0.1, 0.5 and 1 mol%). The powders were placed inside a graphite die using a graphite sheet and two graphite punches. In the next step, they were sintered by applying a pulsed current in a Sinter Land LABOX-100 furnace under vacuum (about 5 Pa) as shown in Fig. 1. At first, the powder in the graphite die was heated to 800 °C by applying the current of 280 A and then held under 10 MPa for 10 min. Next, the sample in the die was heated to 1070 °C at the rate of 90 °C/min by increasing the current to 400 A and then stored for 15 min under 70 MPa. The obtained Ce-doped CaF_2 transparent ceramics were polished for characterization.

The crystallographic structural characterization of the CaF_2 transparent ceramics was performed via X-ray diffraction (XRD) analysis using a Rigaku RINT-2200 V diffractometer. Raman spectra were recorded with a Horiba LabRAM HR Evolution confocal microscope using a 100 mW Nd:YAG laser emitting at 532 nm, 50 % neutral density filter, 100x magnification objective, and 1800 groves/mm diffraction grating. A two-side polished CaF_2 (100) single crystal obtained from MTI Corporation was used as reference. Secondary electron imaging was obtained using a JEOL JCM-6000plus NeoScope scanning electron microscope (SEM). The in-line optical transmittance spectra were recorded using a JASCO V-770 spectrometer. To analyze the photoluminescence (PL) properties, a Shimazu RF-6000 spectrometer was employed to record the PL spectra while a Hamamatsu Photonics Quantaurus-QY spectrometer was used for evaluation of the quantum yields (*QY*). Further, the PL decay was analyzed using a Hamamatsu Photonics Quantaurus-Tau spectrometer.

For the evaluation of scintillation properties, the scintillation spectra under X-ray irradiation were measured using a Andor DU-420-BU2 spectrometer and an optical fiber [36]. To investigate the X-ray induced decay time and afterglow levels, our in-house setup with a pulsed X-ray tube was employed [37]. A photomultiplier tube whose spectral range was 160–650 nm was used in the setup. The pulse height distributions were measured using our measurement system. A Hamamatsu Photonics R7600U-200 photomultiplier tube, a Amptek Pocket MCA multichannel analyzer, a ORTEC Model 113 preamplifer, and a ORTEC model 572 shaping amplifier were used for the measurement of pulse height spectra. Further, an alpha-blocked ^{241}Am radioactive isotope was used as a gamma-ray source (59.5 keV). To evaluate dosimetric properties, the TSL glow curves were recorded using a NanoGray TL-2000 spectrometer. The TSL spectra were determined using a ceramic heater and an Ocean Optics QEPRO spectrometer. Further, the OSL decay curves and OSL spectra were also measured using a JASCO FP-8600 spectrometer.

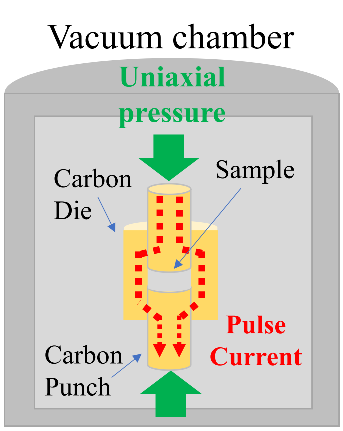

Fig. 1. Schematic diagram of the SPS method.

3. Results and discussion

The visual appearance of the 0.1–1 % Ce-doped CaF_2 transparent ceramics is shown in Fig. 2. The fabricated ceramics were transparent, with the line pattern underneath the ceramics being visible through the ceramics. A few black spots possibly due to carbon contamination were observed. The in-line optical transmittance spectra of the 0.1–1 % Ce-doped CaF_2 transparent ceramics with a thickness of 1 mm are displayed in Fig. 3. The transmittances were 34% (0.1 % CeF_3), 36% (0.5 % CeF_3), and 16% (1 % CeF_3) at 650 nm. The transmittance of the 0.1 and 0.5 % Ce-doped CaF_2 transparent ceramics was comparable to that of the non-doped and Eu-doped CaF_2 ones in our previous studies, and higher than that of the 1 % Ce-doped one [12,30].

Fig. 4(A) presents the XRD patterns of the non-doped and 0.1–1 % Ce-doped CaF_2 transparent ceramics, and the enlarged pattens of the (1 1 1) diffraction peak in the 26–30° of 2-theta range are exhibited in Fig. 4 (B). The observed peaks in Fig. 4(A) agreed well with the previously reported positions for CaF_2, and no peaks associated with secondary phases were observed [38]. Further, the position of the (1 1 1) diffraction peak remained nearly unchanged, regardless of the CeF_3 concentration as exhibited in Fig. 4 (B). This is due to the small

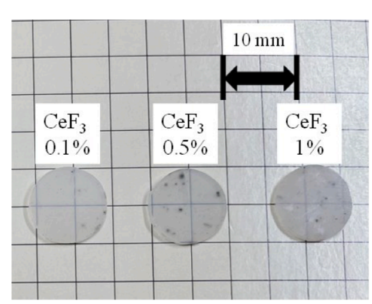

Fig. 2. Visual appearance of the Ce-doped CaF_2 transparent ceramics.

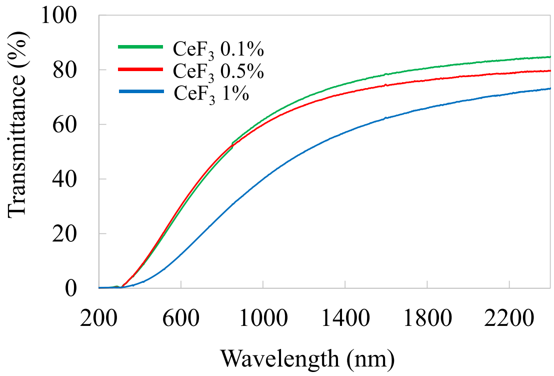

Fig. 3. Transmittance spectra of the Ce-doped CaF_2 transparent ceramics with a thickness of 1 mm.

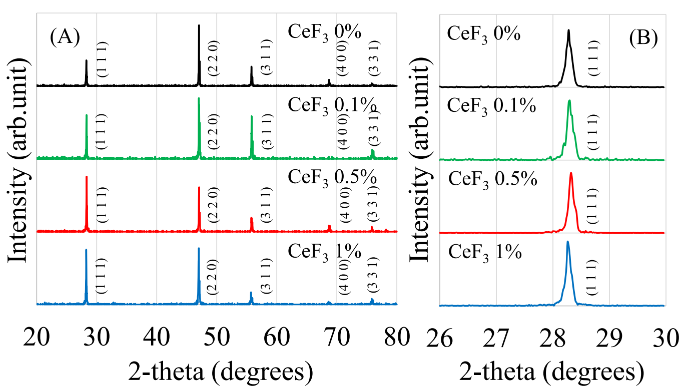

Fig. 4. X-ray diffaraction pattens of undoped and Ce-doped CaF_2 transparent ceramics in the 2-theta range of (A) 20–80° and (B) 26–30°

difference between the ionic radii of Ce^{3+} (1.14 Å) and Ca^{2+} (1.12 Å) in the CaF_2 structure [35].

The Raman spectra of non-doped and 0.1–1 % Ce-doped CaF_2 transparent ceramics are presented in Fig. 5. The Raman spectrum of a non-doped CaF_2 single crystal was also recorded for reference. A single peak at about 320 cm^{-1} assigned to the T_{2g} mode was observed in agreement with previous work [39]. This vibrational mode corresponds to vibrations of F^- ions against each other with Ca^{2+} ions remaining at rest [40]. Structural analysis was evaluated in terms of the peak position and width in comparison to the results from the single crystal (dashed lines). As shown in Fig. 6, a continuous shift to lower peak positions concomitant to an increase of the full width at half maximum (FWHM) up to 0.5 % was observed followed by stabilization. This behavior was interpreted as a progressive increase of structural disorder together with the build-up of internal stress. Due to the small relative difference between the Ca^{2+} and Ce^{3+} ionic radii, less than 2 %, this structural disorder is likely associated to the difference in valence number of these ions and the associated defects created to achieve charge balance.

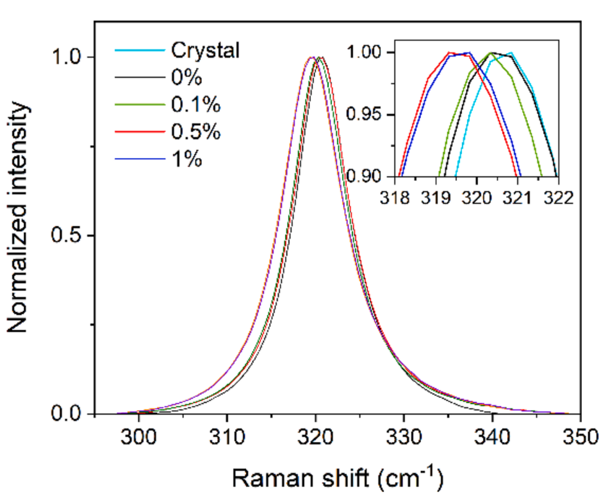

Fig. 5. Partial Raman spectra of the Ce-doped CaF_2 transparent ceramics. The inset highlights the change in peak position.

Fig. 7 shows the SEM images of the 0.1–1 % Ce-doped CaF_2 transparent ceramics. Average grain sizes of the fabricated CaF_2 transparent ceramics were about 20–40 μm, and the size did not change significantly with increasing CeF_3 concentration. The obtained grain sizes for these ceramics were comparable to that (35 μm) of undoped CaF_2 transparent ceramics fabricated by SPS and reported in our previous work [12].

Photoluminescence spectra of the 0.1–1 % Ce-doped CaF_2 transparent ceramics are exhibited in Fig. 8 using 300 nm excitation. Two photoluminescence peaks centered at 323 nm and 346 nm were observed. Based on a previous study, the photoluminescence peaks originated from the 5d→4f transition of Ce^{3+} [9]. Indeed, the difference in energy between these two emission bands was 0.26 eV as expected in Ce^{3+} because of the spin-orbit coupling split of the ground state. Furthermore, a peak at around 386 nm was also detected for the Ce-doped CaF_2 transparent ceramics. This might also be related to the 5d→4f transition of Ce^{3+} [41–43]. When Ce^{3+} ions were incorporated into the CaF_2 host replacing Ca^{2+} ions, the extra charge needed to be compensated. In this study, some of the F^- ions might be replaced by O^{2-} ions possibly due to the presence of trace amounts of oxygen/water in the furnace, forming 'perturbed' Ce^{3+} sites and resulting in the observation of the Ce^{3+} luminescence peak at a longer wavelength in the scintillation spectra [43]. Similar phenomenon was observed in LaF_3: Ce/LaF_3 core-shell nanoparticles [44]. Moreover, the *QYs* of the whole luminescence band within the 320–500 nm range for each ceramic were recorded. The highest *QY* was observed when excited by 310 nm light, and the *QYs* were 38.7% (0.1 % CeF_3), 48.3% (0.5 % CeF_3), and 65.8% (1 % CeF_3), systematically increasing the CeF_3 concentration.

Photoluminescence decay curves of the 0.1–1 % Ce-doped CaF_2 transparent ceramics are shown in Fig. 9. These results were fitted with a single exponential function, and the decay times of each transparent

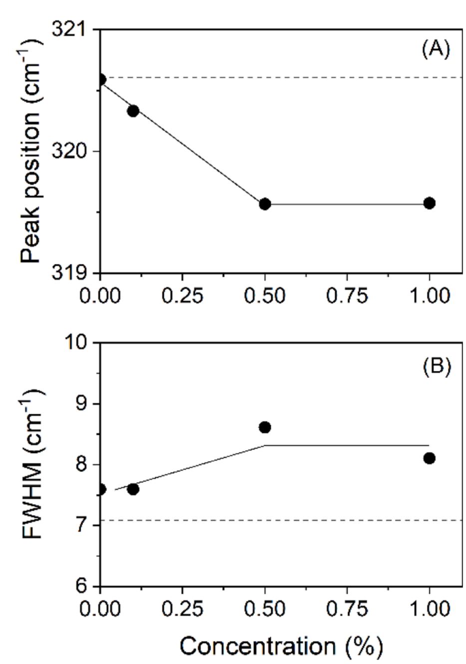

Fig. 6. Raman spectra analysis in terms of (A) peak position, and (B) FWHM, in comparison with the results obtained from a single crystal shown as dashed lines. Continuous lines are guides to the eye only.

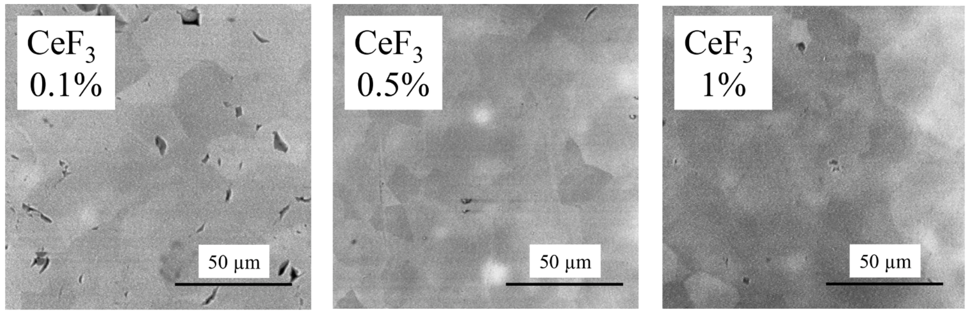

Fig. 7. SEM images of the Ce-doped CaF_2 transparent ceramics.

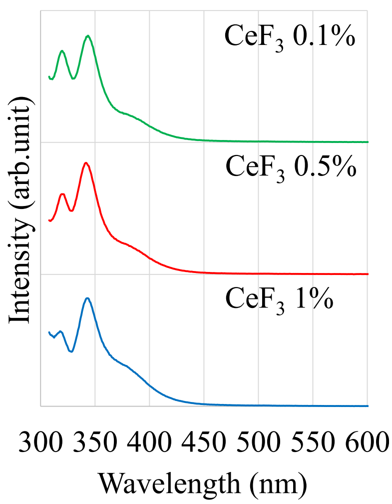

Fig. 8. Photoluminescence spectra of the Ce-doped CaF_2 transparent ceramics.

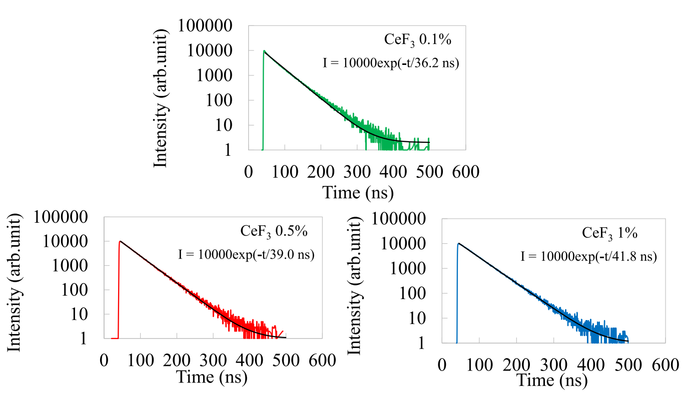

Fig. 9. Photoluminescence decay time profiles of the Ce-doped CaF_2 transparent ceramics under 340 nm light together with their fitting using a single exponential function (black lines).

ceramic were 36.2 ns (0.1 % CeF_3), 39.0 ns (0.5 % CeF_3), and 41.8 ns (1 % CeF_3). These values are comparable with the typical decay time constants of the 5d→4f transition of Ce^{3+} [41,42,44-46].

Fig. 10(A) shows the X-ray induced scintillation spectra of the 0.1–1 % Ce-doped CaF_2 transparent ceramics, and the enlarged spectra within the 200–300 nm range are presented in Fig. 10 (B). A weak peak derived from STE in the CaF_2 host was observed at 293 nm [9]. This emission was sensitive to the incorporation of Ce^{3+}, presenting a significant decrease for higher Ce contents. Further, sharp scintillation peaks appeared at approximately 318 and 345 nm for the Ce-doped CaF_2 transparent ceramics. The scintillation peaks were attributable to the

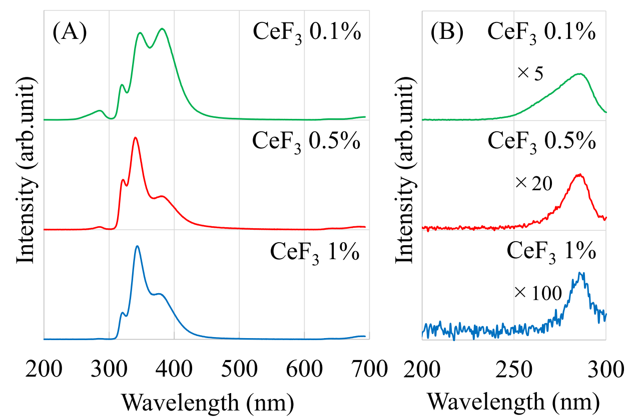

Fig. 10. (A) X-ray induced scintillation spectra of the Ce-doped CaF_2 transparent ceramics, and (B) enlarged spectra in the spectral range of 200–300 nm corresponding to the STE peak.

5d→4f transition of Ce^{3+} according to a previous study [9] and in agreement with our PL results. As in the PL case, emission around 386 nm was also observed and attributed to Ce^{3+} in perturbed sites.

Scintillation decay curves of the 0.1–1 % Ce-doped CaF_2 transparent ceramics obtained by integrating scintillation in the spectral range of 160–650 nm are exhibited in Fig. 11. The decay curves of each transparent ceramic were approximated with a sum of two exponential functions. The first decay times were 45.3 ns (0.1 % CeF_3), 149 ns (0.5 % CeF_3), and 128 ns (1 % CeF_3). This component was ascribed to the 5d→4f transition of Ce^{3+} [41–42]. However, from PL decay measurements, it was determined that the Ce^{3+} lifetime was within 36–42 ns. Consequently, the increase of the scintillation lifetime above these

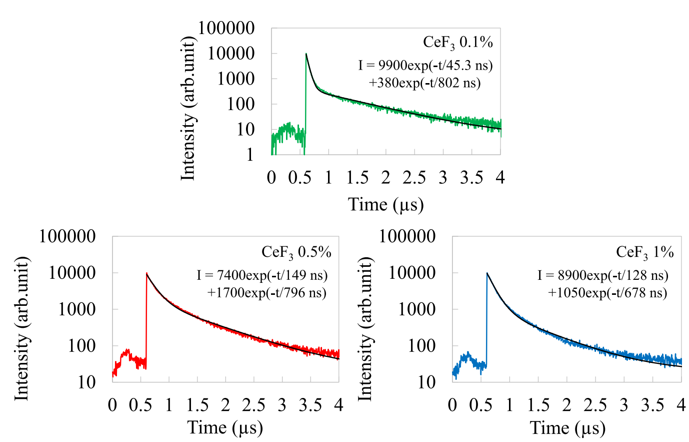

Fig. 11. X-ray induced scintillation decay time profiles of the Ce-doped CaF_2 transparent ceramics together with their fitting using two exponential functions (black lines).

values was interpreted as being related to the transport of the charge carriers (e.g., electrons), more specifically to the trapping and release of the charge carriers by unstable traps. Also, it seemed that this effect was sensitive to the Ce content. For 0.1 % Ce, lifetime was increased by just ~9 ns (when comparing to PL results) while for 0.5 and 1 % the increase was substantial (~86–110 ns). Based on these observations, we speculate the trapping center to be attributed to a defect associated with the incorporation of Ce^{3+}. Further, the second decay times were 802 ns (0.1 % CeF_3), 796 ns (0.5 % CeF_3), and 678 ns (1 % CeF_3). These decay times were similar to the lifetime of STE in the CaF_2 host, suggesting that the origin of this component was STE emission [9].

Fig. 12 shows the pulse height spectra of the 0.1–1 % Ce-doped CaF_2 transparent ceramics under gamma-ray from the alpha-blocked ^{241}Am source. A commercial GS-20 glass scintillator with composition $4Ce_2O_3$–$18Li_2O$–$18Al_2O_3$–$4MgO$–$56SiO_2$ (wt%) was used for reference. Peak channels of the 0.1–1 % Ce-doped CaF_2 transparent ceramics and GS20 were 407 ch (0.1 % CeF_3), 91 ch (0.5 % CeF_3), 87 ch (1 % CeF_3), and 189 ch (GS20). According to the light yield (4000 photons/MeV) of GS20, the light yields were estimated to be 8600 photons/MeV (0.1 % CeF_3), 1930 photons/MeV (0.5 % CeF_3), and 1850 photons/MeV (1 % CeF_3). The photopeaks at lower channels were attributed to the combined low energy gamma-ray emissions of the source. The 0.1 % Ce-doped transparent ceramic showed the largest yield under gamma-ray irradiation, and the light yield was comparable to that of a $Bi_4Ge_3O_{12}$ single crystal [2]. Further, the relationship between QY and scintillation light yield was confirmed. According to theoretical work, the light yield (LY) in the unit of photons/MeV can be expressed by the following formula [1,3,6]:

$$LY\left(\frac{\text{photons}}{\text{MeV}}\right) = \frac{10^6 \times S \times QY}{\beta \times E_g} \tag{1}$$

Here, S is the energy transfer efficiency, E_g is the bandgap, β is a constant (usually $2-3$), and QY is the PL quantum yield as mentioned earlier. According to the bandgap energy of 12 eV for CaF_2 [10], the S values of each transparent ceramic were estimated to be about 0.27β (0.1 % CeF_3), 0.05β (0.5 % CeF_3), 0.03β (1 % CeF_3), indicating that S values decreased with the increase of the CeF_3 concentration. The result is in agreement with the scintillation lifetime analysis that suggested lower charge carrier transport efficiency for higher Ce contents. The S value results suggest that some of the irradiation energy was spent in nonradiative processes. This can be explored for dosimetry applications as discussed later within the context of the analysis of the TSL and OSL results.

The dosimetry properties of the fabricated transparent ceramics were evaluated in terms of TSL and OSL measurements. Fig. 13 shows the TSL glow curves of the 0.1–1 % Ce-doped CaF_2 transparent ceramics. Each ceramic was exposed to X-rays (3 mGy) prior to the TSL measurements. A broad TSL glow peak appeared at around 135 °C (0.1 % CeF_3), 145 °C (0.5 % CeF_3), and 115 °C (1.0 % CeF_3). Among the transparent ceramics, the largest TSL intensity was obtained from the 0.1 % Ce-doped CaF_2 transparent ceramic, and the intensity decreased with the increase of the CeF_3 concentration.

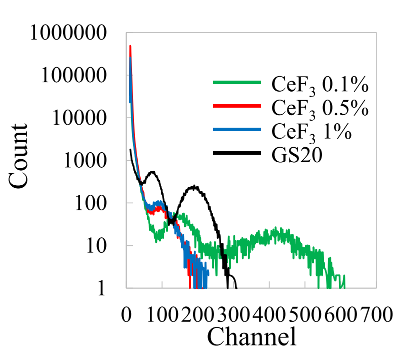

Fig. 12. Pulse height distributions of the Ce-doped CaF_2 transparent ceramics and GS20 glass under gamma-ray irradiation.

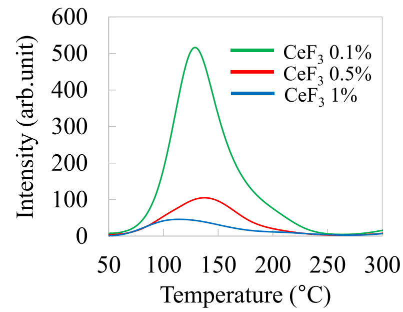

Fig. 13. TSL glow curves of the Ce-doped CaF_2 transparent ceramics at heating rate of 1 °C/s.

The TSL spectra of the 0.1–1 % Ce-doped CaF_2 transparent ceramics are exhibited in Fig. 14. Each ceramic was exposed to X-rays (1 Gy) before the measurement. A broad band from about 300 to 450 nm was observed, and similarly to the scintillation spectra, was attributed to the 5d→4f transition of Ce^{3+}. These results indicated that the recombination center for TSL was Ce^{3+} and modified Ce^{3+} ions in the CaF_2 host.

Moreover, the dose response curves of the 0.1–1 % Ce-doped CaF_2 transparent ceramics were determined in the range of 0.01–3000 mGy using the integrated intensity of the whole glow curves (Fig. 15). The response curves against X-ray irradiation dose showed that the Ce-doped CaF_2 transparent ceramics presented high TSL sensitivity and broad dynamic range. It is possible that they exhibit an even wider range since 0.01 mGy is the lowest detectable dose in the setup used for these measurements due to the restriction of dose delivery and that saturation of the detector occurred just above 3000 mGy. The lowest detectable dose was comparable to that of the commercially available dosimeter Tb-doped Mg_2SiO_4 measured by same evaluation setup [47].

In addition, the OSL properties of the 0.1–1 % Ce-doped CaF_2 transparent ceramics were also evaluated. Fig. 16 shows the OSL emission maps where the broad diagonal line corresponds to the detection of the stimulation light. A broad band centered at around 350 nm appeared when stimulated by 450–600 nm light. This band originated from the 5d→4f transition of Ce^{3+} as per the results reported in Figs. 8 and 10. The OSL intensity of the 0.1 % Ce-doped CaF_2 translucent ceramic was the largest in agreement with the TSL results. Further, the OSL decay curves of the 0.1–1 % Ce-doped CaF_2 transparent ceramics are shown in Fig. 17. The decay curves were fitted with three exponential decay components, and the derived decay times were 2.5 s, 15 s, and 110 s that were essentially invariant regarding the CeF_3 concentration. These results suggested that there were at least three distinct types of detrapping processes in the Ce-doped CaF_2 transparent ceramics. Further, the OSL dose response against the X-ray irradiation dose was evaluated using the intensity of the OSL decay curves at 0 s, and the OSL dose response

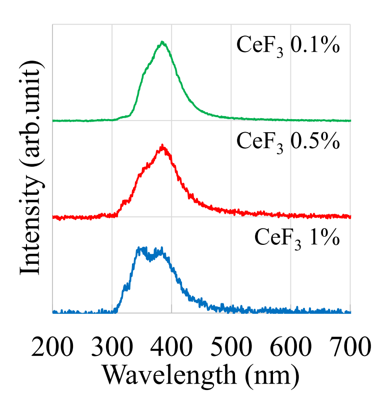

Fig. 14. TSL spectra of the Ce-doped CaF_2 transparent ceramics.

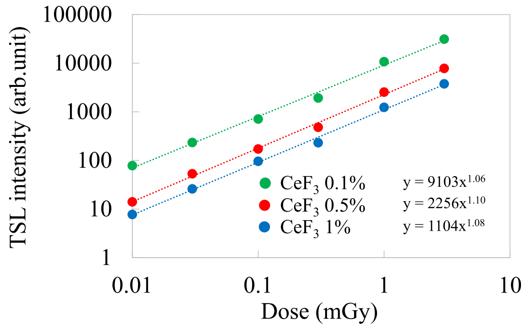

Fig. 15. TSL dose response curves of the Ce-doped CaF_2 transparent ceramics.

curves are presented in Fig. 18. The Ce-doped CaF_2 transparent ceramics showed an almost linear dose response in the range of 0.1–100 mGy, and the minimum detectable dose was estimated to be 0.1 mGy. The minimum dose was comparable to the result of the commercial product Eu-doped BaFBr obtained using same measurement system [48]. As shown in these results, the Ce-doped CaF_2 transparent ceramics were found to exhibit TSL and OSL linear response at low doses. The estimation of radiation dose at low doses is essential for the applications of individual and environmental radiation monitoring such as radiation protection of peoples living in high natural background radiation areas or contaminated areas after nuclear accidents [49–51].

Scintillation efficiency will decrease if the charge carrier mobility decreases (cf. eq. (1)), with the decrease in charge carrier mobility commonly attributed to presence of defects that can trap the charge carriers. Moreover, a larger concentration of traps is associated with a more intense TSL signal. The scintillation light yields and TSL/OSL intensities of the 0.1–1 % Ce-doped CaF_2 transparent ceramics are summarized in Table 1. A direct correlation between the scintillation light yield, TSL and OSL intensities was observed in these ceramics. In some other materials such as Eu-doped $LiCaAlF_6$ crystals, an inverse correlation between the scintillation light yield and the dosimetric signal was demonstrated [8,9]. Since the absorbed energy of the radiation is converted to scintillation signal, dosimetric (TSL and OSL) signal, and thermal energy, this discrepancy may be related to how the absorbed energy is distributed between these channels. It is also important to take into account that not every kind of trap contributes to TSL or OSL though they may affect charge carrier transport efficiency. In this study, the TSL and OSL intensities as well as the scintillation intensity decreased with increasing concentration of CeF_3; therefore, it is likely that the

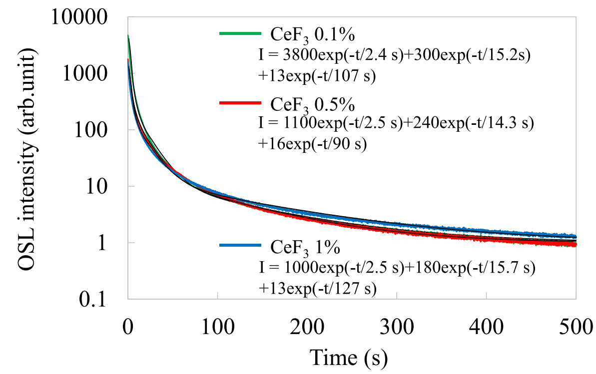

Fig. 17. OSL decay curves of the Ce-doped CaF_2 transparent ceramics under 500 nm light together with their respective fittings (black lines). The monitoring wavelength was 340 nm.

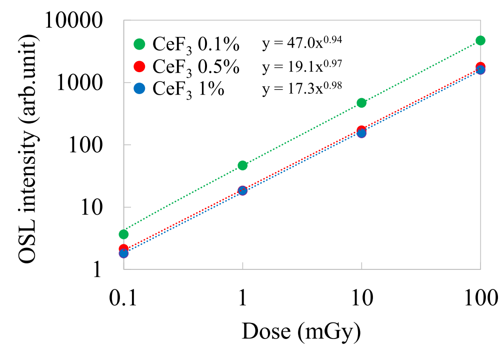

Fig. 18. OSL dose response curves of the Ce-doped CaF_2 transparent ceramics.

Table 1
Scintillation light yield, TSL and OSL intensities of the Ce-doped CaF_2 transparent ceramics.

	Scintillation light yield (photons/MeV)	TSL intensity [3 mGy] (arb.unit)	OSL intensity [10 mGy] (arb.unit)
CeF_3 0.1 %	8600	31,000	470
CeF_3 0.5 %	1930	7800	170
CeF_3 1 %	1850	3800	150

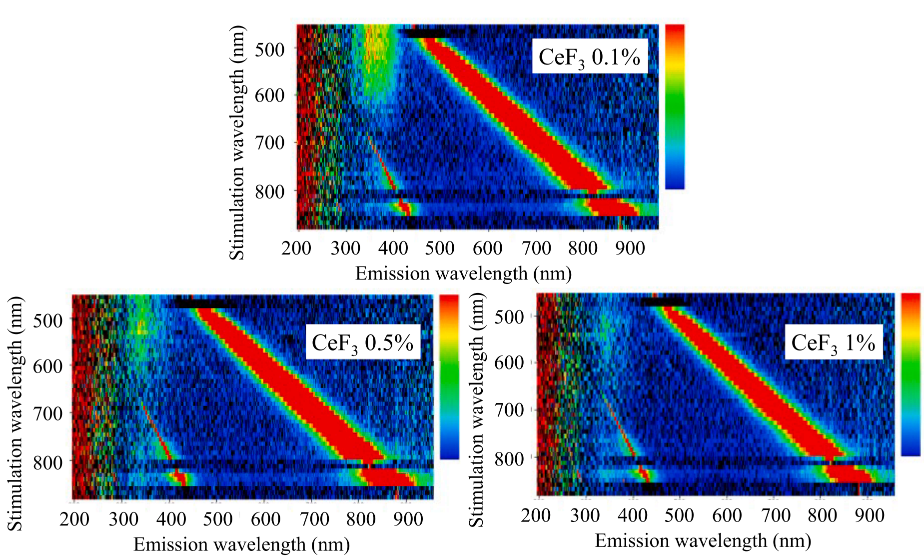

Fig. 16. OSL emission maps of the Ce-doped CaF_2 transparent ceramics.

charge-balancing defects created due to CeF_3 incorporation serve as quenching centers.

4. Conclusions

CaF_2 transparent ceramics with varying CeF_3 concentrations were synthesized, and their luminescence properties were investigated aiming at using these ceramics for ionizing radiation measurements. The Ce-doped CaF_2 transparent ceramics showed emissions derived from the STE and 5d→4f transition of Ce^{3+} under X-ray radiation. The light yield under gamma-ray for the 0.1 % Ce-doped CaF_2 transparent ceramic was about 8000 photons/MeV, similar to BGO, and it decreased for higher CeF_3 concentrations. TSL glow peaks centered at 115–145 °C were observed from the Ce-doped CaF_2 transparent ceramics, and their dose response curves were obtained within the dose range 0.01–3 mGy. Moreover, the Ce-doped CaF_2 transparent ceramics exhibited OSL under 500 nm light. The lowest detectable dose was about 0.1 mGy, and a linear dose response was observed in the dose range from 0.1 mGy to 100 mGy. Interestingly, a direct relationship between scintillation and dosimetry properties was observed in the 0.1–1 % Ce-doped CaF_2 transparent ceramics. Estimates of radiation risks at low doses and low dose rates are important, for example for populations living in contaminated areas after nuclear accidents or in high natural background radiation areas, or for radiation protection of individuals occupationally exposed to ionizing radiation. Within this context, the obtained low detectable limit and dose linearity of TSL and OSL are important for the viewpoint of radiation protection.

CRediT authorship contribution statement

Naoki Kawano: Conceptualization, Investigation, Formal analysis, Writing – review & editing. **Takumi Kato:** Conceptualization, Investigation. **Robin L. Conner:** Investigation, Formal analysis, Writing – review & editing. **Luiz G. Jacobsohn:** Investigation, Formal analysis, Writing – review & editing. **Daisuke Nakauchi:** Investigation. **Yuma Takebuchi:** Investigation. **Hiroyuki Fukushima:** Investigation. **Daiki Shiratori:** Investigation. **Takayuki Yanagida:** Supervision.

Declaration of Competing Interest

The authors declare that they have no known competing financial interests or personal relationships that could have appeared to influence the work reported in this paper.

Data availability

The authors do not have permission to share data.

Acknowledgment

This study is supported by Tohoku Initiative for Fostering Global Researchers for Interdisciplinary Sciences (TI-FRIS) from Japan Science and Technology Agency. L.G. Jacobsohn and R.L. Conner acknowledge support by the National Science Foundation under Grant No. DMR-1653016.

References

[1] T. Yanagida, Inorganic scintillating materials and scintillation detectors, Proc. Jpn. Acad. Ser. B 94 (2018) 75–97.
[2] C.L. Melcher, Scintillators for well logging applications, Nucl. Instrum. Methods Res. Sect. B 40–41 (1989) 1214–1218.
[3] C.W.E. Eijk, Inorganic-scintillator development, Nucl. Instrum. Methods Res. Sect. A. 460 (2001) 1–14.
[4] T. Yanagida, Y. Fujimoto, S. Kurosawa, K. Kamada, H. Takahashi, Y. Fukazawa, Temperature dependence of scintillation properties of bright oxide scintillators for well-logging, Jpn. J. Appl. Phys. 52 (2013), 076401.
[5] J. Glodo, Y. Wang, R. Shawgo, C. Brecher, H. Hawrami, J. Tower, K.S. Shah, New developments in scintillators for security applications, Phys. Procedia 90 (2017) 285–290.
[6] S.E. Derenzo, M.J. Weber, E. Bourret-Courchesne, M.K. Klintenberg, The quest for the ideal inorganic scintillator, Nucl. Instrum. Methods Res. Sect. A. 505 (2003) 111–117.
[7] B.C. Bhatt, Thermoluminescence, optically stimulated luminescence and radiophotoluminescence dosimetry: an overall perspective, Radiat. Prot. Environ. 34 (2011) 6–16.
[8] T. Yanagida, Ionizing radiation induced emission: scintillation and storage-type luminescence, J. Lumin. 169 (2016) 544–548.
[9] T. Yanagida, Y. Fujimoto, K. Watanabe, K. Fukuda, N. Kawaguchi, Y. Miyamoto, H. Nanto, Scintillation and optical stimulated luminescence of Ce-doped CaF_2, Radiat. Meas. 71 (2014) 162–165.
[10] N.M. Trindade, L.G. Jacobsohn, E.M. Yoshimura, Correlation between thermoluminescence and optically stimulated luminescence of α-Al_2O_3:C,Mg, J. Lumin. 206 (2019) 298–301.
[11] H. Shi, R.I. Eglitis, G. Borstel, First-principles calculations of the CaF_2 bulk and surface electronic structure, Phys. stat. sol. 242 (2005) 2041–2050.
[12] F. Nakamura, T. Kato, G. Okada, N. Kawaguchi, K. Fukuda, Yanagida T, Scintillation and dosimeter properties of CaF_2 translucent ceramic produced by SPS, J. Euro. Ceram. Soc. 37 (2017) 1707–1711.
[13] Y. Shimizu, M. Minowa, W. Suganuma, Y. Inoue, Dark matter search experiment with CaF_2(Eu) scintillator at Kamioka Observatory, Phys. Lett. 633 (2006) 195–200.
[14] L.G. Jacobsohn, C.L. McPherson, K.B. Sprinkle, E.G. Yukihara, T.A. DeVol, J. Ballato, Scintillation of rare earth doped fluoride nanoparticles, Appl. Phys. Lett. 99 (2011), 113111.
[15] L.G. Jacobsohn, K.B. Sprinkle, S.A. Roberts, C.J. Kucera, T.L. James, E.G. Yukihara, T.A. DeVol, J. Ballato, Fluoride Nanoscintillators, J. Nanomater. 2011 (2011), 523638.
[16] L.G. Jacobsohn, C.J. Kucera, T.L. James, K.B. Sprinkle, J.R. DiMaio, B. Kokuoz, B. Yazgan Kukouz, T.A. DeVol, J. Ballato, Preparation and characterization of rare earth doped fluoride nanoparticles, Materials (Basel) 3 (2010) 2053–2068.
[17] Data sheet of TLD materials from thermoscientific. https://assets.thermofisher.com/TFS-Assets/LSG/Catalogs/Dosimetry-Materials-Brochure.pdf.
[18] S.F. Wang, J. Zhang, D.W. Luo, F. Gua, D.Y. Tang, Z.L. Dong, G.E.B. Tan, W.X. Que, T.S. Zhang, S. Li, L.B. Kong, Transparent ceramics: processing, materials and applications, Prog. Solid. State. Ch. 41 (2013) 20–54.
[19] A.A. Trofimov, L.G. Jacobsohn, Radioluminescence of $Lu_3Al_5O_{12}$:ce single crystal and transparent polycrystalline ceramic at high temperatures, Ceram. Int. 46 (2020) 26335–26338.
[20] M.G. Chapman, M.R. Marchewka, S.A. Roberts, J.M. Schmitt, C. McMillen, C. J. Kucera, T.A. DeVol, J. Ballato, L.G. Jacobsohn, Luminescence and scintillation enhancement of Y_2O_3:tm transparent ceramic through post-fabrication thermal processing, J. Lumin. 165 (2015) 56–61.
[21] T. Kunikata, T. Kato, D. Shiratori, D. Nakauchi, N. Kawaguchi, T. Yanagida, Scintillation properties of Li-doped ZnO translucent ceramics, Sens. Mater. 34 (2022) 661–668.
[22] H. Kimura, T. Kato, D. Nakauchi, N. Kawaguchi, T. Yanagida, Optical, TSL and OSL properties of copper-doped cesium bromide transparent ceramics prepared by SPS, Sens. Mater. 33 (2021) 2187–2193.
[23] A.A. Trofimov, J.C.A. Santos, D.V. Sampaio, R.S. Silva, T.A. DeVol, L.G. Jacobsohn, Microstructure, luminescence and thermoluminescence of laser-sintered polycrystalline ceramic YAG:ce scintillators, J. Lumin. 251 (2022), 119206.
[24] L.G. Jacobsohn, K. Serivalsatit, C.A. Quarles, J. Ballato, Investigation of Er-doped Sc_2O_3 transparent ceramics by positron annihilation spectroscopy, J. Mater. Sci. 50 (2015) 3183–3188.
[25] P.Y. Poma, K. Upendra Kumar, M.V.D. Vermelho, K. Serivalsatit, S.A. Roberts, C. J. Kucera, J. Ballato, L.G. Jacobsohn, C. Jacinto, Luminescence and thermal lensing characterization of singly Eu^{3+} and Tm^{3+} doped Y_2O_3 transparent ceramics, J. Lumin. 161 (2015) 306–312.
[26] N. Kawano, T. Kato, D. Nakauchi, Y. Takebuchi, H. Fukushima, D. Shiratori, L. G. Jacobsohn, T. Yanagida, TSL, OSL and scintillation properties of Tb-doped barium fluoride translucent ceramics, Opt. Mater. 141 (2023), 113948.
[27] N. Kawano, T. Kato, D. Nakauchi, Y. Takebuchi, H. Fukushima, L.G. Jacobsohn, T. Yanagida, Dosimetric and scintillation properties of Tm-doped BaF_2 translucent ceramics, J. Mater. Sci : Mater. Electron 34 (2023) 962.
[28] Z.W. Zhou, W.W. Li, J.H. Song, B.C. Mei, G.Q. Yi, Y. Yang, Application of Judd-Ofelt theory in analyzing Nd^{3+} doped SrF_2 and CaF_2 transparent ceramics, J. Eur. Ceram. Soc. 39 (2019) 2446–2452.
[29] N. Guo, G. Zhu, H. Xu, X. Jiang, X. Zhang, J. Song, Y. Zhao, K. Jiang, Y. Zhang, Q. Wang, S. Long, T. Wei, A. Yu, Preparation of CaF_2 transparent ceramics by cold sintering, Ceram. Int. 48 (2022) 34184–34189.
[30] F. Nakamura, T. Kato, G. Okada, N. Kawaguchi, K. Fukuda, T. Yanagida, Scintillation and dosimeter properties of CaF_2 transparent ceramic doped with Eu^{2+}, Ceram. Int. 43 (2017) 604–609.
[31] F. Nakamura, T. Kato, G. Okada, N. Kawaguchi, K. Fukuda, T. Yanagida, Scintillation and Dosimeter Properties of CaF_2 Transparent Ceramics Doped with Nd^{3+} Produced by SPS, J. Eur. Ceram. Soc. 37 (2017) 4919–4924.
[32] N. Kawano, D. Nakauchi, F. Nakaumura, T. Yanagida, Scintillation and dosimetric properties of Tb-doped CaF_2 translucent ceramics synthesized by the spark plasma sintering method, J. Asia. Ceram. Soc. 8 (2) (2020) 484–491.
[33] T. Kato, D. Nakauchi, N. Kawaguchi, T. Yanagida, Radio-photoluminescence phenomenon in non-doped CaF_2 ceramic, Mater. Lett. 270 (2020), 127688.
[34] Glenn F. Knoll, Radiation Detection and Measurement, Wiley, 2010, p. 238.

[35] R.D. Shannon, Revised effective ionic radii and systematic studies of interatomie distances in halides and chaleogenides, Acta Cryst. A32 (1976) 751–767.

[36] T. Yanagida, K. Kamada, Fujimoto Y, H. Yagi, T. Yanagitani, Comparative study of ceramic and single crystal Ce:GAGG scintillator, Opt. Mater. 35 (2013) 2480–2485.

[37] T. Yanagida, Y. Fujimoto, T. Ito, K. Uchiyama, K. Mori, Development of X-ray-induced afterglow characterization system, Appl. Phys. Exp. 7 (2014), 062401.

[38] C. Pandurangappa, B.N. Lakshminarasappa, B.M. Nagabhushana, Synthesis and characterization of CaF_2 nanocrystals, J. Alloys. Compd. 489 (2010) 592–595.

[39] A.R. Gee, D.C. O'Shea, H.Z. Cummins, Raman scattering and fluorescence in calcium fluoride, Solid State Commun. 4 (1965) 43–46.

[40] J.A. Koningstein, G. Lucazeau, The Raman spectrum of tetragonal $Eu^{3+}CaF_2$, Chem. Phys. 1 (1973) 112–119.

[41] N. Kawano, N. Kawaguchi, K. Fukuda, G. Okada, T. Yanagida, Scintillation and dosimetric properties of Ce-doped $^{6}LiF/CaF_2$ Eutectic Composites, Opt. Mater. 82 (2018) 60–64.

[42] N. Kawano, N. Kawaguchi, G. Okada, Y. Fujimoto, T. Yanagida, Scintillation and dosimetric properties of Ce-doped strontium aluminoborate glasses, J. Non-Cryst. Solids 482 (2018) 154–159.

[43] S. Chunshan, L. Erbing, Charge compensation and luminous centers in $CaF_2:Ce^{3+}$, J. Alloys. Compd. 192 (1993) 40–41.

[44] L.G. Jacobsohn, A. Toncelli, K.B. Sprinkle, C.J. Kucera, J. Ballato, Spectral engineering of $LaF_3:Ce^{3+}$ nanoparticles: the role of Ce^{3+} in surface sites, J. Appl. Phys. 111 (2012), 074315.

[45] R.E. Muenchausen, L.G. Jacobsohn, B.L. Bennett, E.A. McKigney, J.F. Smith, D. W. Cooke, A novel method for extracting oscillator strength of rare-earth ion optical transitions in nanostructured dielectric materials, Solid Stat. Commun. 139 (2006) 497–500.

[46] L. Pan, J.K.M.F. Daguano, N.M. Trindade, M. Cerruti, E.D. Zanotto, L.G. Jacobsohn, Scintillation, luminescence and optical properties of Ce-doped borosilicate glasses, Opt. Mater. 104 (2020), 109847.

[47] K. Ichiba, Y. Takebuchi, H. Kimura, T. Kato, D. Nakauchi, N. Kawaguchi, T. Yanagida, Analysis of photoluminescence and dosimetric properties of (Ce, Tb)-codoped magnesium orthosilicate single crystals, Sens. Mater. 35 (2) (2023) 475–481.

[48] H. Kimura, T. Kato, T. Fujiwara, M. Tanaka, G. Okada, D. Nakauchi, N. Kawaguchi, T. Yanagida, Optical and photostimulated luminescence properties of Eu:baFBr translucent ceramics synthesized by SPS, Ceram. Int. 49 (2023) 15315–15319.

[49] W. Rühm, T. Azizova, S. Bouffler, H.M. Cullings, B. Grosche, M.P. Little, R.S. Shore, L. Walsh, G.E. Woloschak, Typical doses and dose rates in studies pertinent to radiation risk inference at low doses and low dose rates, J. Radiat. 59 (S2) (2018) ii1–ii10.

[50] W. Rühm, G.E. Woloschak, R.E. Shore, T.V. Azizova, B. Grosche, O. Niwa, S. Akiba, T. Ono, K. Suzuki, T. Iwasaki, N. Ban, M. Kai, C.H. Clement, S. Bouffler, H. Toma, N. Hamada, Dose and dose-rate effects of ionizing radiation: a discussion in the light of radiological protection, Radiat. Environ. Biophys. 54 (2015) 379–401.

[51] B.M. Haley, T. Paunesku, D.J. Grdina, G.E. Woloschak, The increase in animal mortality risk following exposure to sparsely ionizing radiation is not linear quadratic with dose, PLoS ONE 10 (12) (2015), e0140989.